Parametric Study on the Bulk Hydraircooling of Spherical Food Products

K. V. Narasimha Rao, G. S. V. L. Narasimham, and M. V. Krishna Murthy
Dept. of Mechanical Engineering, Indian Institute of Science, Bangalore 560 012, India

A numerical study of the bulk hydraircooling of spherical food products is performed using the technique of spraying chilled water to form a thin film over the food products while blowing cold unsaturated air in the countercurrent or cocurrent direction. This precooling process is found to combine the advantages of hydro- and air cooling.

Governing equations describing the simultaneous heat and mass transfer occurring in the hydraircooling process for both counterflow and parallel-flow arrangements are solved using finite-difference numerical methods. A parametric study is performed to determine the effect of important processing parameters on the process time. It is generally observed that higher quantities of spray water, air-mass flow rate and product thermal conductivity, as well as lower values of water temperature will result in faster rates of cooling. For the same operating conditions, parallel-flow arrangement leads to higher plant capacities.

Introduction

Heat and mass transfer play a very important role in the food processing and preservation methods discussed extensively in surveys (Krishna Murthy and Badarinarayana, 1976; Gaffney et al., 1985). The objective of all food processing and preservation operations is to retard metabolic activity and growth of microorganisms so that the product can be preserved for a longer time. Precooling is one such operation wherein the food products are cooled to storage conditions by rapid removal of field and respiration sources of heat immediately after harvest, collection, or slaughter. Various types of precooling techniques like air cooling, hydrocooling, vacuum cooling, and hydraircooling are discussed in detail in the *ASHRAE Guide and Data Book (Applications)* (1971) and by Hall (1974).

Hydraircooling combines the advantages of both air cooling and hydrocooling. When cold air is passed over the food products that are continuously wetted by a thin film of water, there will be more effective cooling without much moisture loss from the product in comparison to other conventional precooling methods (Abdul Majeed, 1981). This method is therefore especially suited for precooling leafy vegetables like cabbage, lettuce, and so on in which moisture loss is not desirable. This article presents numerical results of a parametric study of heat- and mass-transfer processes occurring during the bulk hydraircooling of spherical food products when the water and air are flowing countercurrent or cocurrent to each other. The governing equations for the product, film, interstitial water spray and the moist air are solved using finite-difference methods. Cooling curves for the food products in various layers are obtained in terms of dimensionless parameters covering a wide range of the product properties and processing conditions encountered in food precooling practice. A sensitivity analysis is performed to bring out the effect of process parameters on the process time for counterflow and cocurrent flow arrangements.

Correspondence concerning this article should be addressed to M. V. Krishna Murthy.

Theoretical Analysis

Description of the physical model

The physical model consists of a number of layers of spherical food products packed in the form of a rectangular parallelepiped (Figure 1). The geometry of the food product is chosen to be spherical, because a large variety of fruits and vegetables can be satisfactorily approximated by this shape. Chilled water is sprayed on to the products in order to produce a thin film of water over each product (Figure 2). The air is

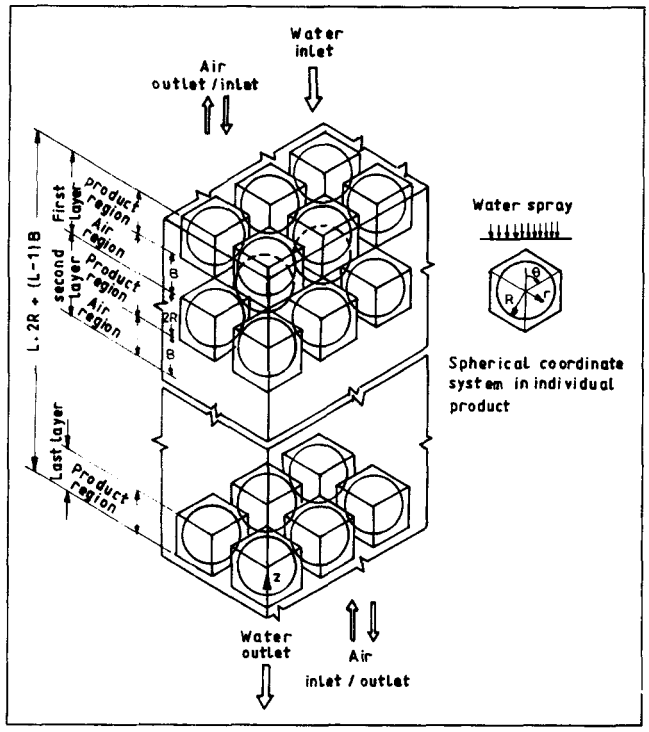

Figure 1. Physical model and coordinate system for bulk hydraircooling of food products.

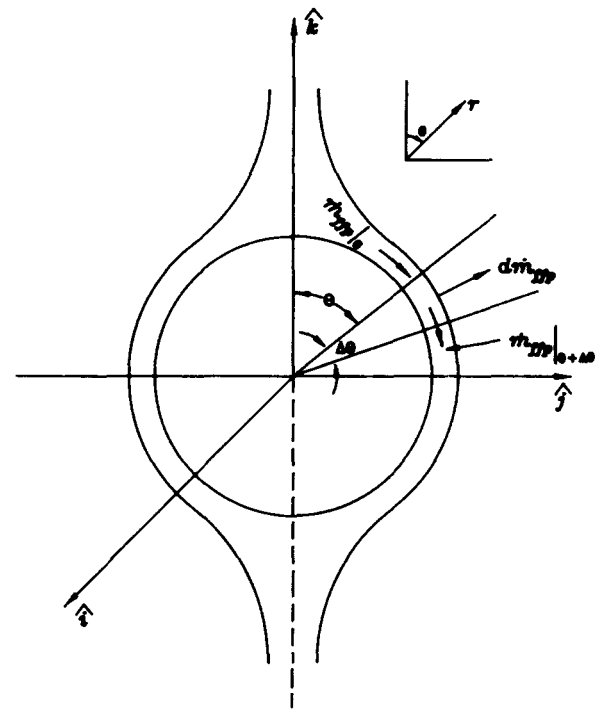

Figure 2. Physical model.

blown from the bottom of the package either in a counterflow direction to that of the water, or in the same direction, resulting in two types of bulk hydraircooling configurations, namely, counterflow and parallel flow. The food products are packed in horizontal layers, one below the other in an in-line arrangement in the vertical direction. The water film, as it flows while enveloping the food product experiences a certain amount of evaporation (from water film surface into the moist air) or condensation (from moist air onto the film surface), depending on the direction of driving potential for mass transfer. When the film approaches the bottom of the product, the water gravitates onto the next food product directly below, forming a film on that product and the process repeats itself. Some of the chilled water, however, is not intercepted by the food products, and falls through the interstitial space of the packing. It is necessary to leave a small air gap between the product layers for ease of loading and unloading in practical situations. If the radius of the product is denoted by R and the height of air gap by B, the overall height of the package, H, containing L product layers will be L.2R + (L − 1)B, as shown in Figure 1. A spherical coordinate system is employed for the food product with the radius r measured from the center of the product while a Cartesian coordinate system is used with z-direction measured from the bottom of the package for the interstitial water spray and the moist air. Thus, for the counterflow process, $z=0$ refers to the inlet for the air and $z=H$ to the outlet and vice versa for the parallel flow.

Initially, all the food products in the package are assumed to be at a uniform temperature T_{po}. The food products are assumed to generate a heat of respiration q_{int}, which is taken to be uniform (space invariant) and constant (time invariant). The package is then exposed at the top of the first layer to a chilled water spray at a temperature of T_{fe}, while cold unsaturated air at a temperature of T_{mae} is blown either from the bottom or from the top of the package depending on the flow arrangement. Water flows as a thin film over any product and gravitates onto the next product directly below in the form of droplets or a liquid column, and larger water flow rates and air gaps give rise to the formation of droplets, as is the case in the present analysis. The heat and mass transfer from these droplets is assumed to be insignificant. This assumption is reasonable, because the interstitial water spray itself is found to have a negligible effect on the cooling process, as explained later in this article. The products are cooled by the combined action of chilled water and air. The conditions of entering water and air are maintained constant throughout in each of the configurations.

Mathematical Formulation

The bulk hydraircooling problem described above involves transient, simultaneous heat and mass transfer. The following assumptions are made in the mathematical formulation of the problem.

Assumptions

(a) The food product is homogeneous and isotropic.

(b) The thermophysical properties of the product are temperature-independent (Lamberg and Hallstrom, 1974).

(c) Moisture concentration gradients and the internal moisture evaporation within the product are ignored (Soule et al., 1966).

(d) The product temperature is invariant in the azimuthal direction.

(e) Air temperature and humidity ratio vary only in the z-direction for both the processes.

(f) Radiation heat transfer is negligible in view of the low ranges of temperatures encountered in precooling practice.

Governing equations

The governing equations are written separately for the product, water film over the product, the interstitial water spray and the moist air. To obtain the solution in a generalized form so that it is applicable to a wide variety of products and processing conditions, the following nondimensionalized variables are defined:

$$a^* = a_p/a_f;\quad a^{**} = a_{ma}/a_f;\quad A_c^* = A_c/R^2\quad A_{fu}^* = A_{fu}R;$$

$$A_{wdu}^* = A_{wdu}R\quad C_p^{**} = C_{pma}/C_{pf};\quad d_{wd}^* = d_{wd}/R\quad Fo = a_p t/R^2;$$

$$Fr_f = [(\dot{m}_{ffpe}/\rho_f R^2)/\sqrt{gR}];\quad H^* = H/R;$$

$$Ja = C_{pf}\Delta T/\Delta h_v;\ \text{where}\ \Delta T = T_{po} - T_{wbe}\quad \dot{m}_{ffe}^* = \dot{m}_{ffe}/\dot{m}_{fe};$$

$$\dot{m}_{fi}^* = \dot{m}_{fi}/\dot{m}_{fe};\quad \dot{m}_{fie}^* = \dot{m}_{fie}/\dot{m}_{fe};\quad \dot{m}_{ma}^* = \dot{m}_{ma}/\dot{m}_{fe};$$

$$Nu_f = \alpha_{hf}2R/\lambda_{ma};\quad Nu_{wd} = \alpha_{hwd}d_{wd}/\lambda_{ma};\quad Pr_f = \nu_f/a_f;$$

$$Pr_{ma} = \nu_{ma}/a_{ma};\quad q_{int}^* = [q_{int}R^2/\lambda_p\Delta T];\quad r^* = r/R;$$

$$R_m = \dot{m}_{ffpe}/\dot{m}_{fe};\quad R_T = T_{wbe}/\Delta T;\quad Re_f = \dot{m}_{ffpe}/\rho_f\nu_f R;$$

$$Re_{mwd} = (w_{wd}\psi \pm w_s)d_{wd}/\nu_{ma}\psi;\quad Re_p = w_s 2R/\nu_{ma};$$

$$Re_{wd} = w_{wd}d_{wd}/\nu_{ma};$$

$$Sc_{ma} = \nu_{ma}/D_{ma};\quad Sh_f = \alpha_{mf}2R/\rho_{ma}D_{ma};\quad Sh_{wd} = \alpha_{mwd}d_{wd}/\rho_{ma}D_{ma};$$

$$T^* = (T - T_{wbe})/\Delta T\quad v_\theta^* = v_\theta/(\dot{m}_{ffpe}/\rho_f R^2);$$

$$y_f^* = y_f/R,\ \text{where}\ y_f = r - R;$$

$$z^* = z/R;\quad \delta^* = \delta/R;\quad \lambda^* = \lambda_p/\lambda_f;\quad \lambda^{**} = \lambda_{ma}/\lambda_f;$$

$$\nu^{**} = \nu_{ma}/\nu_f;\quad \rho^{**} = \rho_{ma}/\rho_f \qquad (1)$$

The governing equations and the corresponding initial and boundary conditions are presented below in dimensionless form.

Dimensionless governing equations: product

The two-dimensional, transient conduction equation as applicable to the product in spherical coordinates is given by

$$\frac{\partial T_p^*}{\partial Fo} = \frac{\partial^2 T_p^*}{\partial r^{*2}} + \frac{2}{r^*}\frac{\partial T_p^*}{\partial r^*} + \frac{\cot\theta}{r^{*2}}\frac{\partial T_p^*}{\partial \theta} + \frac{1}{r^{*2}}\frac{\partial T_p^{*2}}{\partial \theta^2} + q_{int}^* \qquad (2)$$

Liquid film

The coordinate system for the liquid film is shown in Figure 2. In view of the thinness of the film ($\mu_f\rho_f \gg \mu_{ma}\rho_{ma}$), the transverse pressure gradient is neglected, and since the impressed pressure on the film is assumed to be constant, the streamwise pressure gradient becomes zero. The governing equation for the momentum in the liquid film with a quasi-steady approximation is written as follows:

$$\frac{d^2 v_\theta^*}{dy_f^{*2}} = -\frac{Re_f}{Fr_f^2}\sin\theta \qquad (3)$$

The above equation is written under the assumption that the viscous forces balance the gravitational forces, which is the case if acceleration terms are negligible (for example, Chyu and Bergles, 1987).

Energy equation:

$$\frac{\partial T_f^*}{\partial Fo} + \frac{v_\theta^* Re_f Pr_f}{a^*}\frac{\partial T_f^*}{\partial \theta} = \frac{1}{a^*}\left(\frac{1}{\delta^{*2}}\frac{\partial^2 T_f^*}{\partial y_f^{*2}} + \frac{\partial^2 T_f^*}{\partial \theta^2}\right) \qquad (4)$$

Mass conservation:

$$\frac{d\dot{m}_{ffp}^*}{d\theta} = -\frac{Sh_f}{2Re_f Sc_{ma}}\nu^{**}\rho^{**}2\pi\sin\theta(W_{sf} - W_{ma}) \qquad (5)$$

Water spray

Mass conservation equation:

$$\frac{d\dot{m}_{fi}^*}{dz^*} = \frac{Sh_{wd}\rho^{**}\nu^{**}A_{wdu}^* A_c^* R_m}{Re_f Sc_{ma} d_{wd}}(W_{swd} - W_{ma}) \qquad (6)$$

Here A_{wdu}^* denotes the area of water droplets available per unit volume of the package. The determination of this quantity requires the diameter of the water droplet and the number of water droplets contained in unit volume of the package. In this investigation an average droplet diameter of 0.85 mm and an average droplet velocity of 10 $m\cdot s^{-1}$ are used (Ranz and Marshall, 1952). These assumptions, however, have little influence on the final results, as discussed later in the results and discussion section. The value of A_{wdu}^* can then be calculated as follows:

If N is the number of water droplets present per unit volume of the package, for an interstitial water spray mass-flow rate of $\dot{m}_{fie}$, average droplet diameter of d_{wd}, and a superficial velocity of w_{wd}, N is given by,

$$N = 6\frac{\dot{m}_{fie}R}{\pi\rho_f d_{wd}^3 w_{wd}}\quad \text{where}\quad \dot{m}_{fie} = 0.5(3\psi - 1.0)\dot{m}_{fe} \qquad (7)$$

$$\text{Thus,}\ A_{wdu} = N\pi d_{wd}^2/A_c R \qquad (8)$$

$$A_{wdu}^* = 3.0(3\psi - 1.0)Re_f Pr_f/\pi Re_{wd} a^{**} Pr_{ma} \qquad (9)$$

Energy equation:

$$\frac{\partial T^*_{wd}}{\partial Fo} - \frac{Re_{wd}\nu^{**}Pr_f}{a^* d^*_{wd}}\frac{\partial T^*_{wd}}{\partial z^*} = \frac{Re_{wd}Sh_{wd}\rho^{**}\nu^{**2}A^*_{wdu}A^*_c Pr_f R_m}{Re_f Sc_{ma} d^{*2}_{wd} a^* \dot{m}^*_{fi}}(T^*_{wd}+R_T)(W_{swd}-W_{ma}) - \frac{Re_{wd}Nu_{wd}\lambda^{**}\nu^{**}A^*_{wdu}A^*_c R_m}{Re_f d^{*2}_{wd} a^* \dot{m}^*_{fi}}(T^*_{swd}-T^*_{ma}) - \frac{Re_{wd}Sh_{wd}\rho^{**}\nu^{**2}A^*_{wdu}A^*_c Pr_f R_m(1+Ja)}{Ja\, Re_f Sc_{ma} d^{*2}_{wd} a^* \dot{m}^*_{fi}}(W_{swd}-W_{ma}) \quad (10)$$

Moist air

In the following energy and species conservation equations for moist air, counter- and parallel-flow configurations are represented by a single equation by prefixing a $\pm$ sign to the convective terms. The plus sign refers to counterflow and the minus sign refers to parallel flow.

The equation for the conservation of energy in the moist air is written as follows:

$$\psi\frac{\partial T^*_{ma}}{\partial Fo} \pm \frac{\dot{m}^*_{ma}Re_f Pr_f}{\rho^{**}A^*_c a^* R_m}\frac{\partial T^*_{ma}}{\partial z^*} = \psi\frac{a^{**}}{a^*}\frac{\partial^2 T^*_{ma}}{\partial z^{*2}} + \frac{Nu_f a^{**}A^*_{fu}}{2a^*}(T^*_{sf}-T^*_{ma}) + \frac{Nu_{wd}a^{**}A^*_{wdu}}{d^*_{wd}a^*}(T^*_{swd}-T^*_{ma}) \quad (11)$$

where ψ is the void fraction which is defined as the volume of the void to that of the package in any product layer. ψ assumes a value of 1.0 in the region in between the food layers. Also, the first heat source term (that is, the second term in the righthand side) in the above equation vanishes in this region.

The equation for the conservation of water vapor in the moist air can be written as follows:

$$\psi\frac{\partial W_{ma}}{\partial Fo} \pm \frac{\dot{m}^*_{ma}Re_f Pr_f}{\rho^{**}A^*_c a^* R_m}\frac{\partial W_{ma}}{\partial z^*} = \frac{Pr_f\nu^{**}}{Sc_{ma}a^*}\psi\frac{\partial^2 W_{ma}}{\partial z^{*2}} + \frac{Sh_f Pr_f A^*_{fu}\nu^{**}}{2Sc_{ma}a^*}(W_{sf}-W_{ma}) + \frac{Sh_{wd}Pr_f A^*_{wdu}\nu^{**}}{Sc_{ma}a^* d^*_{wd}}(W_{swd}-W_{ma}) \quad (12)$$

As explained earlier, ψ assumes a value of 1.0 and the first mass source term (that is, the second term in the righthand side) vanishes in the air-water spray region.

Initial and boundary conditions: product and film

The initial uniform temperature of the product gives the following condition:

$$Fo \le 0, \text{ for } 0 \le r^* \le 1.0 \text{ and } 0 \le \theta \le \pi,\ T^*_p = 1.0 \quad (13)$$

$$T^*_p \text{ remains finite as } r^* \text{ tends to } 0 \quad (14)$$

The continuity of the heat flux and the condition of no temperature jump at the product-film interface gives the following condition:

$$\text{At } r^* = 1.0, \text{ for } 0<\theta<\pi,\ \lambda^*\frac{\partial T^*_p}{\partial r^*}\bigg|_{r^*=1} = \frac{\partial T^*_f}{\partial y^*_f}\bigg|_{y^*_f=0} \text{ and } T^*_p = T^*_f = T^*_{if} \quad (15)$$

where T^*_{if} is the product-film interface temperature.

Symmetry of the temperature profile about the vertical axis yields:

$$\text{At } \theta = 0 \text{ and } \theta = \pi \text{ and } Fo > 0 \text{ for } 0 < r^* < 1.0,\ \frac{\partial T^*_p}{\partial \theta} = 0 \quad (16)$$

The boundary conditions for the film momentum equation (Eq. 3) are written as follows:

$$\text{At } y^*_f = 0,\ v^*_\theta = 0, \text{ and,} \quad (17)$$

$$\text{at } y^*_f = \delta^*,\ \frac{dv^*_\theta}{dy^*_f} = 0 \quad (18)$$

The assumption of initially uniform temperature of the water film results in the following condition:

$$\text{For } Fo \le 0,\ 0 \le y^*_f \le \delta^* \text{ and } 0 \le \theta \le \pi,\ T^*_f = T^*_{fo} \quad (19)$$

At the surface of the liquid film which is in contact with the air, the energy transfer takes place due to the combined effect of heat and mass transfer. The temperature difference between the film surface and the free stream air acts as the driving force for the sensible heat transfer, whereas the vapor pressure difference causes evaporation of water at the film surface resulting in the transfer of latent heat. This boundary condition in terms of the sensible and latent heat transfers, after simplification, is written as follows:

$$\text{At } y^*_f = \delta^* \text{ and } 0 \le \theta \le \pi,\ -\frac{\partial T^*_f}{\partial y^*_f} = B_0 + B_1 T^*_{sf} + B_2 T^{*2}_{sf} \quad (20)$$

where B_0, B_1, and B_2 are defined as shown below:

$$B_0 = -\frac{Nu_f\lambda^{**}T^*_{ma}}{2} + \frac{Sh_f Pr_{ma}\lambda^{**}}{2Sc_{ma}C^{**}_p Ja}(C_0 - W_{ma})$$

$$B_1 = -\frac{Nu_f\lambda^{**}}{2} + \frac{Sh_f Pr_{ma}\lambda^{**}}{2Sc_{ma}C^{**}_p Ja}C_1$$

$$B_2 = \frac{Sh_f Pr_{ma}\lambda^{**}}{2Sc_{ma}C^{**}_p Ja}C_2 \quad (21)$$

In the above boundary conditions, C_0, C_1, and C_2 are the coefficients in the quadratic expression for saturated humidity ratio at the film surface in terms of its temperature and are as follows:

$$W_{sf} = C_0 + C_1 T^*_{sf} + C_2 T^{*2}_{sf} \quad (22)$$

where

$$C_0 = A_0 + A_1 R_T \Delta T + A_2 R_T^2 \Delta T^2$$

$$C_1 = A_1 \Delta T + 2A_2 R_T \Delta T^2$$

$$C_2 = A_2 \Delta T^2 \tag{23}$$

where A_0, A_1 and A_2 are the coefficients of a second degree polynomial expressing the humidity ratio of saturated air in terms of its temperature as follows:

$$W_s = A_0 + A_1 T_s + A_2 T_s^2 \tag{24}$$

The values of constants A_0, A_1, and A_2 are given below for a temperature range of 0–20°C.

$$A_0 = 3.879 \times 10^{-3} \text{ (dimensionless)}$$

$$A_1 = 2.173 \times 10^{-4} \text{ °C}^{-1}$$

$$A_2 = 1.605 \times 10^{-5} \text{ °C}^{-2} \tag{25}$$

A continuous supply of spray water at T^*_{fe} is assumed to be available for the top layer to maintain a film of flowing water. This gives the condition:

$Fo > 0$, at $\theta = 0$ and $0 < y^*_f < \delta^*$, $T^*_f = T^*_{fe}$ (first layer) or T^*_{fbm} (subsequent layers) (26)

Here, T^*_{fbm} represents the bulk mean temperature of the water collected at the bottom of the preceding food product. The value of $T^*_{fbm}|_\theta$ at any θ is calculated from the following expression for any particular layer.

$$T^*_{fbm} = \left\{ \frac{1}{\dot{m}^*_{ffp}} \int_0^{\delta^*} 2\pi v^*_\theta \sin\theta T^*_f (1 + y^*_f) dy^*_f \right\} \tag{27}$$

The outflow boundary condition on temperature for the film is written as:

$$\text{at } \theta = \pi \text{ and } 0 \le y^*_f \le \delta^*, \quad \frac{\partial T^*_f}{\partial \theta} = 0 \tag{28}$$

Water spray

$$\text{At } z^* = H^*, \ \dot{m}^*_{fi} = \dot{m}^*_{fie} = 1.0 - \dot{m}^*_{ffe} \tag{29}$$

$$Fo = 0, \text{ for } 0 \le z^* \le H^*, \ T^*_{wd} = T^*_{fe} \tag{30}$$

$$Fo > 0, \text{ at } z^* = H^*, \ T^*_{wd} = T^*_{fe} \tag{31}$$

Moist air

For the moist air, initial conditions are the same for both counter and parallel flows. However, the boundary conditions are to be prescribed at the respective inlet and the exit of the package as explained in the physical model.

$$\text{At } Fo = 0, \text{ for } 0 \le z^* \le H^*, \ T^*_{ma} = T^*_{mae} \text{ and } W_{ma} = W_{mae} \tag{32}$$

For $Fo > 0$, at the inlet: ($z^* = 0$ for counterflow and $z^* = H^*$ for parallel flow)

$$T^*_{ma} = T^*_{mae} \text{ and } W_{ma} = W_{mae} \tag{33}$$

At the outlet: ($z^* = 0$ for counterflow and $z^* = H^*$ for parallel flow):

$$\frac{\partial T^*_{ma}}{\partial z^*} = 0 \text{ and } \frac{\partial W_{ma}}{\partial z^*} = 0 \tag{34}$$

The Nusselt number and the Sherwood number in Eq. 21 are evaluated using the following equations (Beukema et al., 1982):

$$Nu_f = 1.27(1 - \psi)^{0.41} Re_p^{0.59} Pr_{ma}^{0.33}$$

$$Sh_f = 1.27(1 - \psi)^{0.41} Re_p^{0.59} Sc_{ma}^{0.33}, \text{ for } Re_p > 180 \tag{35}$$

The following correlations are used to determine the Nusselt number and the Sherwood number at the water droplet surface (Bird et al., 1960):

$$Nu_{wd} = 2.0 + 0.6\ Re_{mwd}^{0.5} Pr_{ma}^{0.33}$$

$$Sh_{wd} = 2.0 + 0.6\ Re_{mwd}^{0.5} Sc_{ma}^{0.33} \tag{36}$$

After finding the air dry bulb temperature, T^*_{ma}, and the humidity ratio, W_{ma}, the wet bulb temperature is determined by solving the following equation in dimensionless form (*ASHRAE Handbook of Fundamentals*, 1989)

$$D_1 T^{*3}_{wb} + D_2 T^{*2}_{wb} + D_3 T^*_{wb} = D_4 \tag{37}$$

where

$$D_1 = 2.381 C_2 \Delta T$$

$$D_2 = 2.381 C_1 \Delta T + 2.381 C_2 R_T - 2{,}501 C_2$$

$$D_3 = 2.381 C_0 \Delta T + 2.381 C_1 R_T \Delta T - 2{,}501 C_1 - \Delta T - 4.186\ \Delta T W_{ma}$$

$$D_4 = 2{,}501 C_0 - 2.381 C_0 R_T \Delta T - T^*_{ma} \Delta T - 2{,}501 W_{ma} + 2.381 R_T \Delta T W_{ma} - 1.805 T^*_{ma} \Delta T W_{ma} \tag{38}$$

Method of Solution

The following expressions for the film thickness (δ^*), and the tangential velocity (v^*_θ) are obtained by solving the film momentum equation (Eq. 3)

$$\delta^* = \left(\frac{3 Fr_f^2 \dot{m}^*_{ffp}}{2\pi \sin^2 \theta Re_f} \right)^{1/3} \tag{39}$$

$$v^*_\theta = \frac{Re_f}{Fr_f^2} \sin\theta \delta^{*2} \left(\frac{y^*_f}{\delta^*} - \frac{1}{2} \frac{y^{*2}_f}{\delta^{*2}} \right) \tag{40}$$

The dimensionless governing equations for the product, film, water spray, and moist air (Eqs. 2–6 and 10–12) along with the initial and boundary conditions (Eqs. 13–20, Eq. 26, and Eqs. 28–34) are solved using finite-difference techniques.

In view of the symmetry about the vertical axis due to negligible temperature variation in the azimuthal direction, a semicircular region containing the product and the film is

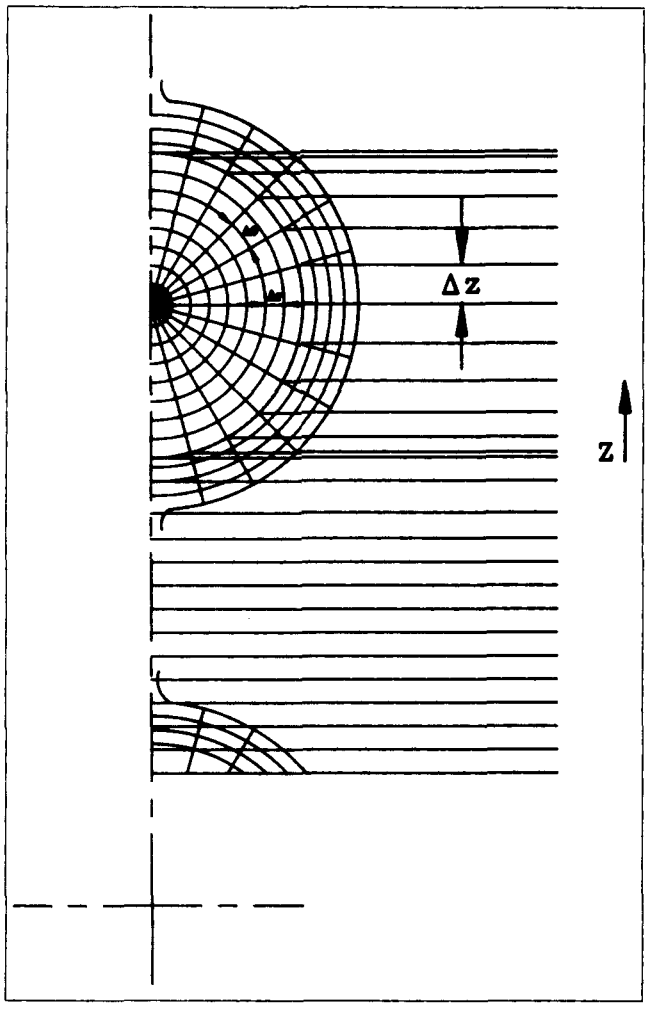

Figure 3. Finite difference grid system for the product, film, and the accompanying air-spray region.

considered as the computational domain. The computational domain and the layout of the finite-difference grid are shown in Figure 3. For simplicity only one product layer with the adjacent air gap is shown in the figure. A nonuniform grid is adopted for the solution of moist air and water spray in the interstices between the products. This nonuniform grid is obtained by horizontally extending the radial lines ending on the product surface. In the region between the product layers, a uniform grid is chosen.

The Peaceman-Rachford Alternating Direction Implicit (ADI) procedure (Peaceman and Rachford, 1955) with forward-time centered-space (FTCS) differencing is employed to simultaneously advance the temperatures in the product and the film from time Fo to $Fo+\Delta Fo$ (that is, from time level 'n' to '$n+1$'). The ADI procedure accomplishes this task in two halftime steps. In the first halftime step, the equation is implicit in the r-direction while in the second halftime step, it is implicit in the θ-direction giving rise at each halftime step to a simple tridiagonal system of linear-algebraic equations.

The discretized forms of the product and the film energy equations (Eq. 2 and Eq. 4) for the first halftime-step are as follows.

Product equation:

$$(T_p^{*(n+1/2)} - T_p^{*(n)})/(\Delta Fo/2) = (T_{p,l+1}^{*(n+1/2)} - 2T_{p,l}^{*(n+1/2)} + T_{p,l-1}^{*(n+1/2)})/(\Delta r^*)^2 + (T_{p,l+1}^{*(n+1/2)} - T_{p,l-1}^{*(n+1/2)})/(r_l^* \Delta r^*) + \cot\theta_m (T_{p,m+1}^{*(n)} - T_{p,m-1}^{*(n)})/(2(r_l^*)^2 \Delta\theta) + (T_{p,m+1}^{*(n)} - 2T_{p,m}^{*(n)} + T_{p,m-1}^{*(n)})/(r_l^* \Delta\theta)^2 + q_{\text{int}}^* \quad (41)$$

where $r_l^* = (l-1)\Delta r^*$, and $\theta_m = (m-1)\Delta\theta$.

Here the subscripts l and m pertain to r and θ-directions respectively ($l=1$ represents the center and $m=1$ represents the line $\theta=0$). The default subscripts not indicated in the above equation should be taken appropriately. Thus, for instance, $T_{p,l+1}^{*(n+1/2)}$ should actually read $T_{p,l+1,m}^{*(n+1/2)}$.

The above equation can be rearranged to yield the following form:

$$A_l^p T_{p,l-1}^{*(n+1/2)} + B_l^p T_{p,l}^{*(n+1/2)} + C_l^p T_{p,l+1}^{*(n+1/2)} = D_l^p \quad (42)$$

where

$$A_l^p = -1/(\Delta r^*)^2 + 1/(r_l^* \Delta r^*)$$

$$B_l^p = (2/\Delta Fo) + 2/(\Delta r^*)^2$$

$$C_l^p = -1/(\Delta r^*)^2 - 1/(r_l^* \Delta r^*)$$

$$D_l^p = E_m^p T_{p,m-1}^{*(n)} + F_m^p T_{p,m}^{*(n)} + G_m^p T_{p,m+1}^{*(n)} + q_{\text{int}}^{*(n)} \quad (43)$$

where

$$E_m^p = -\cot\theta_m/(2(r_l^*)^2\Delta\theta) + 1/(r_l^*\Delta\theta)^2$$

$$F_m^p = (2/\Delta Fo) - 2/(r_l^*\Delta\theta)^2$$

$$G_m^p = \cot\theta_m/(2(r_l^*)^2\Delta\theta) + 1/(r_l^*\Delta\theta)^2 \quad (44)$$

Liquid film equation:

$$(T_f^{*(n+1/2)} - T_f^{*(n)})/(\Delta Fo/2) + (Re_f Pr_f/a^*) v_{\theta,l}^* (T_{f,m}^{*(n)} - T_{f,m-1}^{*(n)})/\Delta\theta = (1/a^*)[(T_{f,m+1}^{*(n)} - 2T_{f,m}^{*(n)} + T_{f,m-1}^{*(n)})/(\Delta\theta)^2 + (T_{f,l+1}^{*(n+1/2)} - 2T_{f,l}^{*(n+1/2)} + T_{f,l-1}^{*(n+1/2)})/(\delta_m^{*(n+1/2)} \Delta y_f^*)^2] \quad (45)$$

The above equation, on rearrangement, yields the following equation:

$$A_l^f T_{f,l-1}^{*(n+1/2)} + B_l^f T_{f,l}^{*(n+1/2)} + C_l^f T_{f,l+1}^{*(n+1/2)} = D_l^f \quad (46)$$

where

$$A_l^f = -1/[a^*(\Delta y_f^* \delta_m^{*(n+1/2)})^2]$$

$$B_l^f = (2/\Delta Fo) + 2/[a^*(\Delta y_f^* \delta_m^{*(n+1/2)})^2]$$

$$C_l^f = A_l^f$$

$$D_l^f = E_m^f T_{f,m-1}^{*(n)} + F_m^f T_{f,m}^{*(n)} + G_m^f T_{f,m+1}^{*(n)} \quad (47)$$

where

$$E_m^f = (Re_f Pr_f v_{\theta,1}^*)/[a^*(\Delta\theta)] + 1/[a^*(\Delta\theta)^2]$$

$$F_m^f = (2/\Delta Fo) - (Re_f Pr_f v_{\theta,1}^*)/(a^*\Delta\theta) - 2/[a^*(\Delta\theta)^2]$$

$$G_m^f = 1/[a^*(\Delta\theta)^2] \tag{48}$$

The interface boundary condition, Eq. 15 at the product-film interface applicable to $(n+1/2)$ time level, can be discretized as below:

$$\lambda^*(T_{p,if}^{*(n+1/2)} - T_{p,if-1}^{*(n+1/2)})/\Delta r^* = (T_{f,if+1}^{*(n+1/2)} - T_{f,if}^{*(n+1/2)})/(\delta_m^{*(n+1/2)}\Delta y_f^*) \tag{49}$$

The nonlinear boundary condition at the film surface, Eq. 20 is linearized and discretized to yield:

$$T_{sf}^{*(n+1/2)} = E_1 + E_2 T_{sf-1}^{*(n+1/2)} \tag{50}$$

where $E_1 = P/Q$, $E_2 = 1/Q$
where

$$P = -\delta_m^{*(n+1/2)}\Delta y_f^*[B_0 - B_2(T_{sf}^{*(n)})^2]$$

$$Q = 1 + \delta_m^{*(n+1/2)}\Delta y_f^*[B_1 + 2B_2(T_{sf}^{*(n)})] \tag{51}$$

This linearization is similar to the one employed for radiation boundary conditions (Carslaw and Jaeger, 1959) and is justified in view of the small temperature differences involved. The boundary conditions at $\theta = 0$ and π (Eqs. 16 and 28) are discretized using two-point one-sided differences.

Equations 42 and 46, when applied to the product and film regions on a radial line along with the interface boundary condition (Eq. 49) and the boundary condition at the film surface (Eq. 50) and the nth level center temperature, form a set of linear-algebraic equations of tridiagonal form which can be solved using the Thomas algorithm (von Rosenberg, 1969). After sweeping all the radial lines ($m = 2$ to the second-to-last), the temperatures on the lines $\theta = 0$ and $\theta = \pi$ are calculated. This completes the calculation for the first halftime step.

A similar procedure is used for the second halftime step with the appropriate finite difference equations.

Owing to the nonexistence of radial symmetry at the center of the food product the radial gradient cannot be prescribed at the center. Therefore, to calculate the product center temperature, a local Cartesian mesh is used as was employed by Hwang and Cheng (1970) with the applicable equation being:

$$\frac{\partial T_p^*}{\partial Fo} = \frac{\partial^2 T_p^*}{\partial X^{*2}} + \frac{\partial^2 T_p^*}{\partial Y^{*2}} + \frac{\partial^2 T_p^*}{\partial Z^{*2}} + q_{int}^* \tag{52}$$

The coordinates X, Y, and Z in the above equation are measured from the center of the spherical food product. The discretized form of the above equation gives the center temperature in terms of the temperatures at its six nearest neighboring points, four of them (lying in the plane $\theta = \pi/2$) being equal. Thus, the center temperature can finally be related to the temperatures of the neighboring points on the lines $\theta = 0$, $\theta = \pi/2$, $\theta = \pi$.

The bulk mean temperature of the film, T_{fbm}^*, given by Eq. 27, is then calculated using Simpson's rule at the adjacent station to $\theta = \pi$, and this serves as the entry temperature of water to the next product layer. In this manner, the product and film energy equations are solved for all the layers.

The mass conservation equation for the water spray (Eq. 6) is solved using a simple marching method. The energy equations for the water spray, moist air and the water vapor conservation equation (Eqs. 10, 11, and 12) are one-dimensional transient equations. The FTCS differencing is adopted for these equations except for the convective terms for which upwind differences are used (Roache, 1982). The discretization of these equations is quite straightforward but lengthy and therefore is not presented here. These equations are also solved using the tridiagonal matrix algorithm mentioned above.

The finite difference analogues for the second derivatives occurring in the above equations should take into account the nonuniform grid spacing. If F denotes either T_{ma}^* or W_{ma}^*, and $\Delta z_k^* = \Delta z_{k+1}^* - \Delta z_k^*$, the second derivative F'' with respect to z^* at the grid point k can be written as shown below.

$$F_k'' = 2[(\Delta z_k^*/\Delta z_{k-1}^*)F_{k-1} - (1 + \Delta z_k^*/\Delta z_{k-1}^*)F_k + F_{k+1}]/[\Delta z_k^*(\Delta z_k^* + \Delta z_{k-1}^*)] \tag{53}$$

The source terms appearing in the discretized equations are evaluated at the time level 'n' wherever necessary.

A number of numerical experiments are performed to determine the grid size and the time step for which the numerical solutions are stable and grid-independent. Various grids with the number of grid points ranging from 13 to 41 in r-direction (combined product and film region) and from 15 to 37 in θ-direction with time steps of 0.0005, 0.001, 0.0025, 0.004, and 0.005 are examined. A total number of 60 numerical experiments are performed to determine the grid size and the time step. Finally, a grid size of 41 × 37 and a time step of 0.001 have been found to give accurate solutions. The selection of grid size in the product and the film region automatically fixes the number of grid points in the moist air region of the product layer and the interstitial water spray in the z-direction, as can be visualized from Figure 3. An equal number of uniformly spaced grid points are employed in the accompanying air gaps. All the computations are performed on the computer system CYBER 992. A typical run covering a dimensionless process time of 1.0 took about 600 s of CPU time for packages consisting of 10 product layers. It may be noted that a dimensionless process time ($Fo = a_p t/R^2$) of 1.0 corresponds to 80 min of physical process time for an average value of $a_p = 1.3 \times 10^{-7}$ m^2·s^{-1} and for a typical product radius of 0.025 m.

The nondimensionalization of the governing equations and the initial and boundary conditions shows that a number of parameters govern the problem of heat and mass transfer in bulk hydraircooling. The parameters of the problem are:

$$a^*,\ a^{**},\ A_c^*,\ C_0,\ C_1,\ C_2,\ C_p^{**},\ d_{wd}^*,\ Fr_f,$$

$$Ja,\ L,\ \dot{m}_{ma}^*,\ Pr_f,\ Pr_{ma},\ q_{int}^*,\ Re_f,\ Re_{wd},$$

$$Sc_{ma},\ T_{fe}^*,\ T_{mae}^*,\ W_{mae},\ \psi,\ \lambda^*,\ \lambda^{**} \text{ and } \rho^{**} \tag{54}$$

The parameters A_{fu}^*, A_{wdu}^*, $\dot{m}_{fic}^*$, Nu_f, Nu_{wd}, R_m, R_T, Re_p,

Re_{mwd}, Sh_f, Sh_{wd}, and ν^{**} are not independent parameters as these are expressible in terms of other independent parameters listed above as follows:

$$A^*_{fu} = 3.0(1.0 - \psi) \tag{55}$$

$$R_m = \pi / A^*_c \tag{56}$$

$$Re_{mwd} = Re_{wd} \pm 0.5 Re_p \, d^*_{wd} \psi \tag{57}$$

$$Re_p = 2.0 \dot{m}^*_{ma} Re_f / \pi \nu^{**} \rho^{**} \tag{58}$$

$$\nu^{**} = a^{**} Pr_{ma} / Pr_f \tag{59}$$

The parameters $\dot{m}^*_{fie}$ and A^*_{wdu} are given by Eqs. 7 and 9. R_T is a function of ΔT, T^*_{mae}, and W_{mae} and is obtained by solving the following cubic equation:

$$S_1 R_T^3 + S_2 R_T^2 + S_3 R_T + S_4 = 0 \tag{60}$$

where

$$\begin{aligned} S_1 &= 2.381 A_2 \Delta T^3 \\ S_2 &= 2.381 A_1 \Delta T^2 - 2{,}501 A_2 \Delta T^2 \\ S_3 &= 2.381 A_0 \Delta T - 2.381 \Delta T W_{mae} - 2{,}501 A_1 \Delta T \\ S_4 &= 2{,}501 A_0 - T^*_{mae} \Delta T - 2{,}501 W_{mae} - 1.805 T^*_{mae} \Delta T W_{mae} \end{aligned} \tag{61}$$

The quantities Nu_f, Sh_f, Nu_{wd} and Sh_{wd} can be calculated using the Eqs. 35 and 36.

Among the independent parameters, the quantities a^{**}, C_p^{**}, Pr_f, Pr_{ma}, Sc_{ma}, λ^{**} and ρ^{**} become fixed for the air-water system. a^* also is fixed because most of the fruits and vegetables have more or less the same value of thermal diffusivity (*ASHRAE Handbook of Fundamentals*, 1989) and hence a^* can be taken to be a constant.

The parameters C_0, C_1, C_2, and Ja can be considered to be fixed once the difference between the product initial temperature and the air wet bulb temperature at the entry (ΔT) is specified. The dimensionless cross-sectional area of the test section, A^*_c, is assumed to be constant in the present analysis. Since the water droplet diameter and its average velocity are assumed to be constant, the parameters d^*_{wd} and Re_{wd} also become fixed.

Even after limiting the parameters thus, it may be noted that there remain as many as ten parameters to be varied in the present analysis. Numerical solutions are obtained for the following values of the parameters so as to cover a wide range of fruits and vegetables and precooling conditions of practical interest:

T^*_{fe} is varied from 0.05 to 0.22. This corresponds to the entering spray water temperature ranging from 4.5 to 10°C.

Re_f is varied from 5.0 to 60.0 in steps of 5.0. This corresponds to an entering water mass flow rate of 0.017 to 0.204 $kg \cdot s^{-1}$ for the test section having a cross-sectional area of 0.25 m^2.

$\dot{m}^*_{ma}$ is varied from 0.1 to 12.0. This corresponds to air velocity of 0.017 to 2.04 $m \cdot s^{-1}$ for a film Reynolds number of 30.0.

T^*_{mae} is varied from 0.075 to 0.25.

W_{mae} is varied from 0.0023 to 0.005.

λ^* is varied from 0.3 to 0.7 in steps of 0.05. This corresponds to product thermal conductivity of 0.1755 to 0.4095 $W \cdot m^{-1} \cdot K^{-1}$, the thermal conductivity of water being 0.585 $W \cdot m^{-1} \cdot K^{-1}$. These values cover a wide range of thermal conductivity values for common fruits and vegetables (*ASHRAE Handbook of Fundamentals*, 1989).

ψ is varied from 0.5 to 0.95 in steps of 0.05.

L is varied from 1 to 65 in steps of 1.

q^*_{int} is varied from 0.0015 to 0.012. This corresponds to heat of respiration values of 26 $W \cdot m^{-3}$ to 208 $W \cdot m^{-3}$ applicable to common fruits and vegetables.

Fr_f is varied from 0.0014 to 0.007 in steps of 0.0014.

In addition, the following parameters are held constant at the values indicated:

- product-water thermal diffusivity ratio, $a^* = 0.9136$
- air-water thermal diffusivity ratio, $a^{**} = 137.5$
- area of cross-section of the package, $A^*_c = 400.0$
- air-water specific heat ratio, $C_p^{**} = 0.2402$
- water droplet diameter, $d^*_{wd} = 3.4 \times 10^{-2}$
- water Prandtl number, $Pr_f = 7.8798$
- moist air Prandtl number, $Pr_{ma} = 0.7482$
- mass-flow rate ratio, $R_m = 7.854 \times 10^{-3}$
- moist air Schmidt number, $Sc_{ma} = 0.6654$
- air-water thermal conductivity ratio, $\lambda^{**} = 4.214 \times 10^{-2}$
- air-water density ratio, $\rho^{**} = 1.2727 \times 10^{-3}$ (62)

Results and Discussion

Typical time-temperature histories during bulk hydrair-cooling

Figures 4 and 5 show typical cooling curves for different layers in packages consisting of 15 product layers for counterflow and parallel flow processes respectively for identical values of processing conditions. It can be seen that the cooling

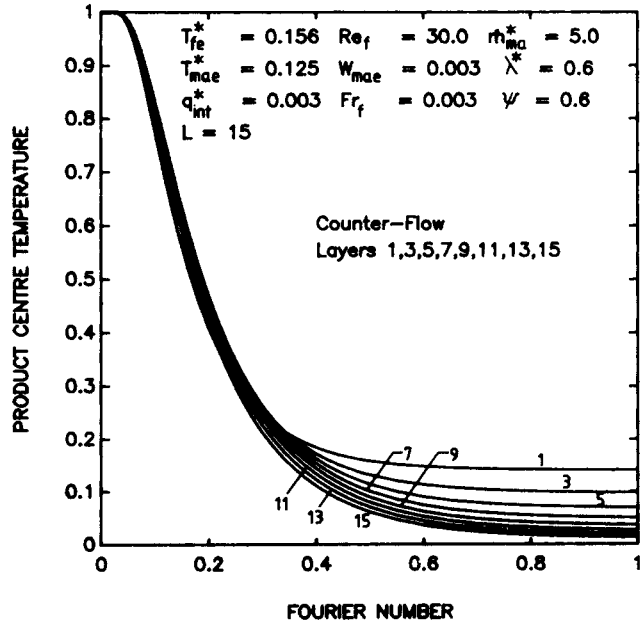

Figure 4. Typical cooling curves during bulk hydrair-cooling-counterflow process.

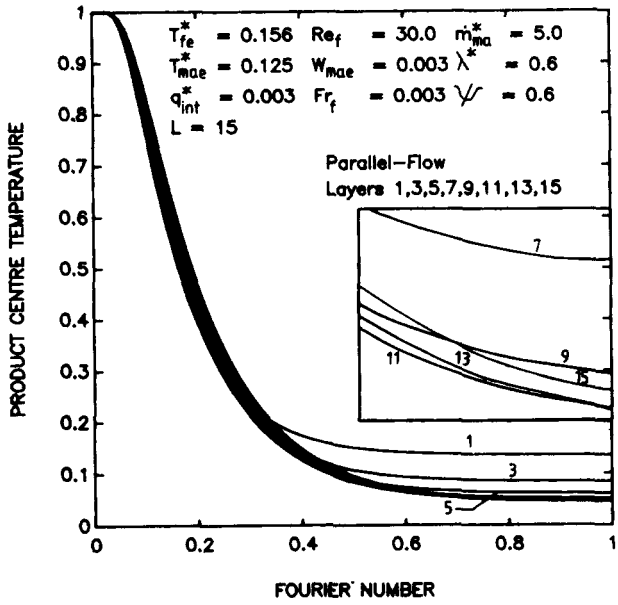

Figure 5. Typical cooling curves during bulk hydrair-cooling-parallel-flow process.

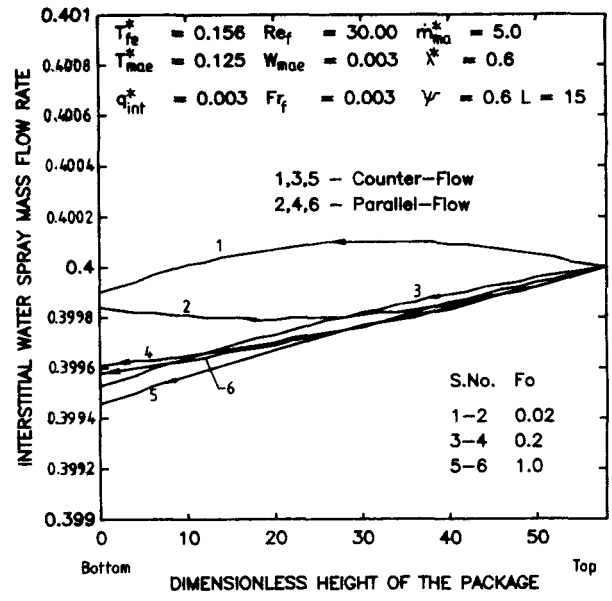

Figure 6. Variation of interstitial water spray mass-flow rate.

rate is almost the same for all the layers until a certain time. However, after a reasonably long time, different layers reach different steady-state temperatures. This trend is explained as follows:

The food products in any layer are cooled by the water film enveloping it and the film in turn is cooled by the surrounding moist air. Thus, the heat transfer takes place from the products to the film and from the film to the moist air. Up to a certain time (about 0.2 for the parameters chosen in Figures 4 and 5), these two heat-transfer rates balance each other and hence the food products in all the layers are in contact with the water film at more or less the same temperature.

However, at larger times this trend changes. In the bottom layers, for countercurrent arrangement (Figure 4), the film comes into contact with already cooled products and the simultaneous heat and mass transfer from the water film to the air further reduces the temperature of the already cooled film as it flows down the package. This results in lower steady-state temperatures for the bottom layers.

In parallel flow (Figure 5), the food products in the top layer always come into contact with spray water at the temperature T^*_{fe} ($T^*_{fe} = 0.156$) and the air at the entry conditions ($T^*_{mae} = 0.125$ and $W_{mae} = 0.003$), which are favorable conditions for the same to cool faster until a certain time has elapsed. The other layers, however, cool slower than the first layer initially, the reason being the nonestablishment of the evaporative cooling during that relatively small time. As time progresses, the evaporative cooling becomes effective in the subsequent layers whose cooling rate exceeds that of the top layer and thus the crossover of cooling curve of the first layer occurs in parallel flow. As can be expected, steady-state temperature of the top layer is about 0.14, which is only slightly less than that of the entering water while the bottom layers reach much lower steady-state temperatures.

The bottom layers (say, layers 11 to 15) are found to reach very nearly the same steady-state temperature which is slightly lower than that of the seventh layer for the parameters prescribed. Among layers 11 to 15, the steady-state temperatures attained by the food products are progressively higher towards the bottom of the package as can be seen from the inset of Figure 5. This is because of the fact that the moist air becomes relatively hotter and more humid while passing through these layers and thereby becomes less effective in cooling the film.

Another interesting trend that can be noticed by comparing Figures 4 and 5 is regarding the range of the steady-state temperatures obtained by different layers. Counterflow process yields final temperatures ranging from 0.013 to 0.141. These correspond to actual temperatures of 3.4 to 7.5°C, where as parallel-flow process results in values of 0.046 to 0.135, which correspond to 4.4 to 7.3°C. This shows that the parallel-flow arrangement cannot yield as low a steady-state temperature as the counterflow arrangement for some of the layers (especially the bottommost layers).

Figure 6 shows that there is a very small variation of interstitial water spray mass-flow rate along the height of the package for both the parallel and counterflow arrangements. This means that there is a negligible evaporation or condensation from the surface of the water droplets.

Figure 7 shows the variation of interstitial water spray temperature as it passes along the package. At smaller times, the interstitial water spray temperature is seen to first increase and then decrease, due to condensation on and evaporation from the surface of water droplets (depending on the enthalpy difference between the surface of the water droplets and the surrounding moist air, which is the driving potential for the combined sensible and latent heat transfer). The opposite trend is observed for the parallel-flow arrangement at smaller times. Even a small quantity of water evaporating from or condensing over the surface of the water droplets causes considerable decrease or increase in its temperature owing to the large value of enthalpy of evaporation associated with water. However, at larger times, the water spray temperature monotonically

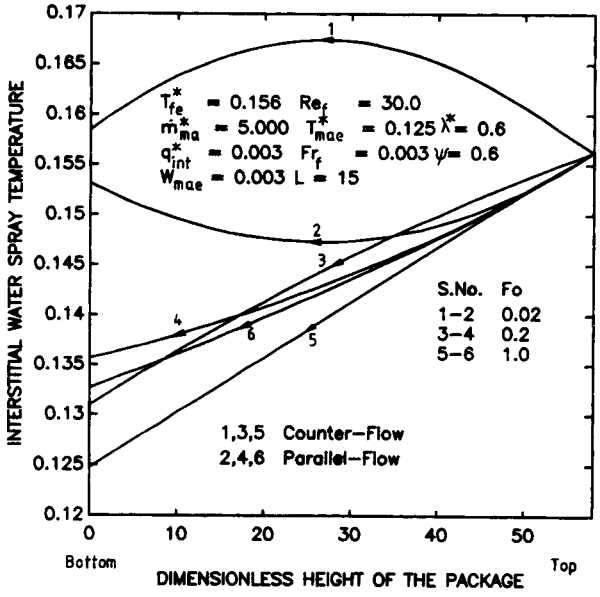

Figure 7. Variation of interstitial water spray temperature.

decreases for either arrangement, with the counterflow process always yielding a lower temperature at the bottom of the package.

Figure 8 shows the variation of air dry bulb temperature as it passes through the package. It is observed that for both counter- and parallel-flow configurations, the air temperature increases with distance quite appreciably at initial times and tends to decrease at larger times. The air temperature varies almost linearly as it passes through the product layers and is more or less constant in the intervening space. This is due to the fortuitous property of a sphere by which its surface area varies linearly along any diametral axis. The air may pick up from and/or dissipate heat to the water film and water droplets. The film has a very large surface area whereas the water droplet

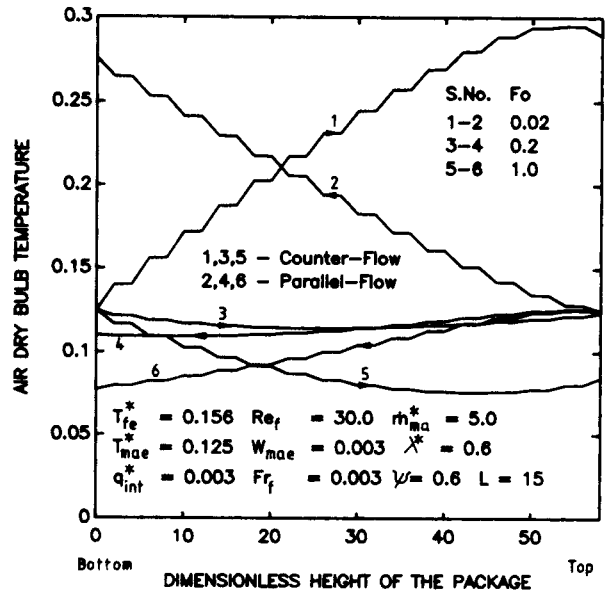

Figure 8. Typical variation of air dry bulb temperature.

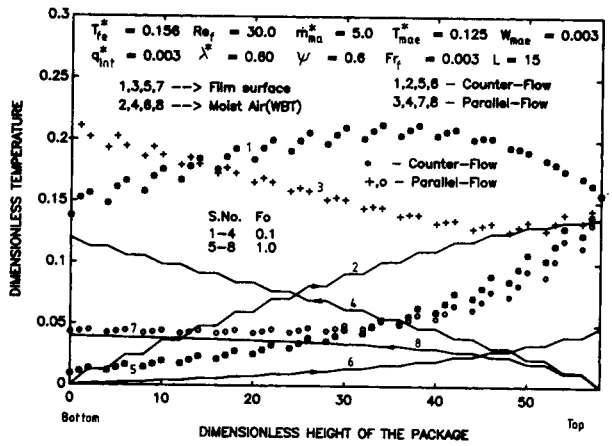

Figure 9. Typical variation of film surface and air temperatures.

has a relatively smaller surface area. In fact, the film surface area (A^*_{fu}) is two orders of magnitude higher than the surface area of water droplets (A^*_{wdu}) and hence the relative contribution from the surface of water droplets is very small.

Figure 9 shows the variation of film surface and the air wet bulb temperatures along the height of the package at different times. Air wet bulb temperature varies much the same way as its dry bulb temperature (Figure 8) except that it will not decrease from its initial value ($T^*_{wbe} = 0.0$ at the air inlet) at any point in space as well as time. The film gets heated up due to heat transfer from the food products. At smaller times, the film surface temperature increases continuously along the length of the package for parallel-flow whereas it increases for certain distance and then decreases for counterflow process. This is due to the effect of cold and unsaturated air entering from the bottom of the package in the case of counterflow. After steady-state conditions are reached, the film actually cools slightly by exchanging energy with the moist air.

Figure 10 shows the typical variation of air humidity ratio

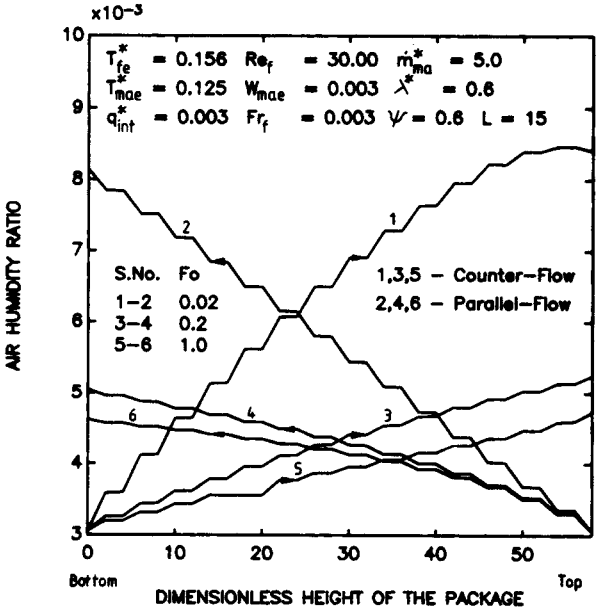

Figure 10. Typical variation of air humidity ratio.

as it passes through the package. It is observed that the air is becoming more humid while passing through the package, especially in the product layers. Because of the large film surface area available for evaporation to take place, the entering air which is cold and unsaturated picks up moisture, and the moisture pick up is higher in the product layers than in the product-free layers. The increase in the air humidity ratio becomes less at larger times both for counter- and parallel-flows.

Process time

Process time is the time for which the hydraircooling is to be carried out to obtain the storage temperature suitable for the product prior to transport. The storage temperature is different for different fruits and vegetables. However, for food products such as apples, cabbage and lettuce, a storage temperature of about 10°C will be sufficient. In the present investigation, a dimensionless product temperature of 0.2 is considered as the maximum allowable storage temperature. This corresponds typically to a temperature of 9.4°C for an initial product temperature of 35°C and entering air wet bulb temperature of 3°C. Also, since the food products in different layers reach different steady-state temperatures depending on the processing conditions, the layer that takes the maximum time for reaching the storage temperature is taken as the basis for determining the process time for that set of parameter values.

Effect of different parameters on bulk hydraircooling

Figure 11 shows the effect of entering water temperature on the process time for both counterflow and parallel-flow arrangements. It can be observed that higher values of water temperature result in higher process times. This is obvious because higher values of water temperature mean smaller temperature differences between the product and the cooling medium, thereby causing lower cooling rates. It can also be seen that for lower values of water temperature ($T^*_{fe} = 0.06$ to 0.09), counterflow and parallel-flow configurations yield equal process times where as for water temperatures higher than 0.09 (corresponding to 5.9°C) parallel-flow arrangement yields lower process times.

Figure 12 shows the effect of film Reynolds number on the bulk hydraircooling. It can be seen that higher values of film Reynolds number result in faster cooling rates up to a value of about 20.0. It does not seem to have much influence at still higher values. A higher value of film Reynolds number for a fixed value of product diameter means a larger water flow rate. It is seen that Eq. 4, for very high values of Re_f ($Re_f \to \infty$) merely reduces to $\partial T_f/\partial\theta \simeq 0$, which means that there is no tangential variation of the film temperature. Also, Eq. 5 shows that the evaporation is quite insignificant at such large water mass-flow rates. The products in any layer cool as if they were being subjected to a constant temperature at their surface equal to the entry water temperature. The problem reduces to simple cooling of a sphere in a stream of water with a very large heat-transfer coefficient (Biot number $\to \infty$). A T^*_{pc} of 0.2 and a T^*_{fe} of 0.156 as per the present definitions would correspond to a T^*_{pc} of 0.052 as per the definition of nondimensional temperature of Heisler's charts. The time-temperature variation of the products can therefore be obtained from the one-dimensional transient conduction charts like those of Heisler available in any standard textbook on Heat Transfer (for example, Holman, 1986). For this, a value of about 0.4 for the Fourier number can be read from the chart which compares fairly with the asymptotic value of the process time of about 0.35 for either arrangement. There is nothing much to choose between the two processes based on the film Reynolds number.

Figure 13 shows the effect of mass-flow rate of air on bulk hydraircooling. It is seen that higher values of mass-flow rate of air result in lower process times in both the configurations, but the curves become flatter for $\dot{m}^*_{ma}$ values exceeding about 5.0. This behavior can be explained by noting that a higher

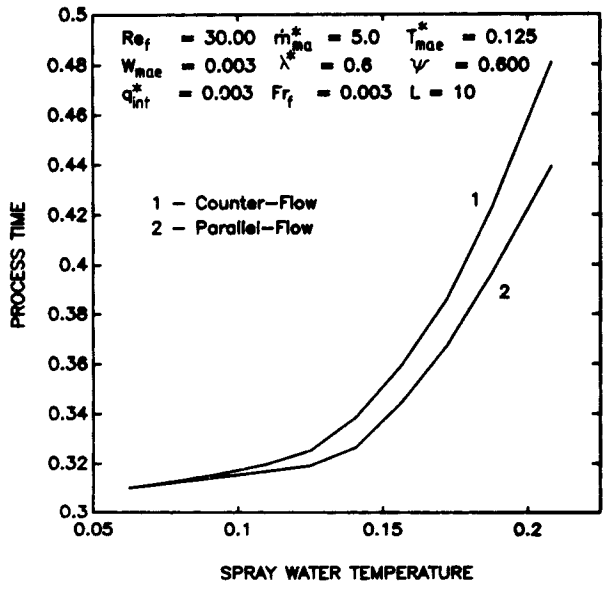

Figure 11. Effect of spray water temperature on bulk hydraircooling.

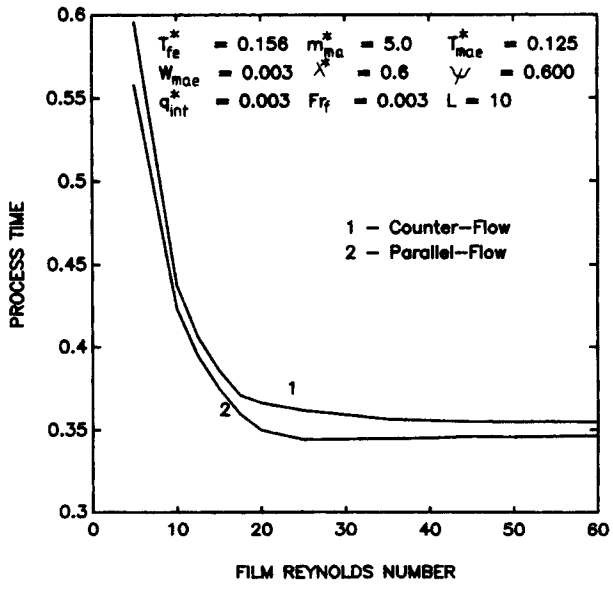

Figure 12. Effect of film Reynolds number on bulk hydraircooling.

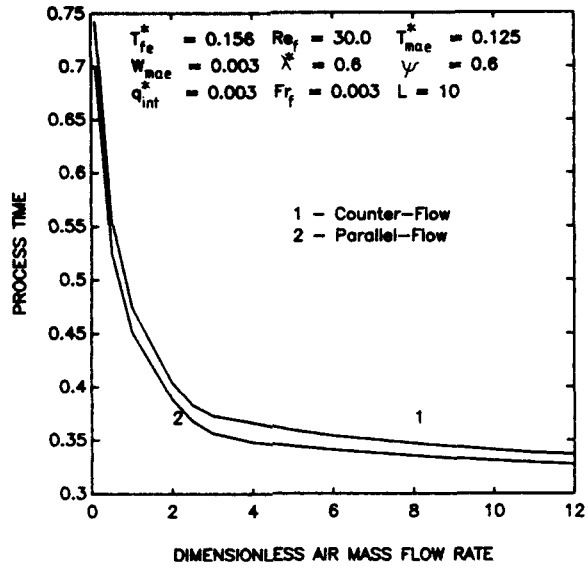

Figure 13. Effect of air mass-flow rate on bulk hydraircooling.

value of air mass-flow rate is always accompanied by higher heat and mass-transfer coefficients from the film surface resulting in lower process times. However, the gain in terms of the process time is not appreciable beyond a certain value of air mass-flow rate. At such high air mass-flow rates, the presence of water film does not have any effect and therefore, the process time appears to approach the value for forced air-precooling. These asymptotic values can again be obtained from the Heisler's charts. A Fourier number of 0.37 can be read for a T^*_{pc} of 0.2, and a T^*_{mae} of 0.125 (Biot number $\rightarrow \infty$) while Figure 13 shows process times of 0.33 and 0.34 for parallel and counterflow arrangements, respectively, both of which agree closely with the value obtained from Heisler's charts. This close agreement shows that at very high air mass-flow rates, the products seem to approach the one-dimensional transient cooling with constant temperature boundary condition.

Tables 1 and 2 show respectively the effect of dimensionless entering air dry bulb temperature and humidity ratio on bulk hydraircooling. The dimensionless process time varies only in the third decimal place for both counter and parallel flows.

Table 1. Effect of Dimensionless Entering Air Dry Bulb Temperature on Bulk Hydraircooling

Case	T^*_{mae}	Process Time	
		Counterflow	Parallel-flow
1	0.075	0.3600	0.3478
2	0.1	0.3596	0.3460
3	0.125	0.3593	0.3431
4	0.15	0.3582	0.3431
5	0.175	0.3572	0.3419
6	0.2	0.3563	0.3407
7	0.225	0.3554	0.3397
8	0.25	0.3546	0.3387

$T^*_{fe} = 0.156$; $Re_f = 30.0$; $\dot{m}^*_{ma} = 5.0$; $W_{mae} = 0.003$; $\lambda^* = 0.6$; $\psi = 0.6$; $L = 10$; $q^*_{int} = 0.003$; $Fr_f = 0.0028$; $\Delta T = 32.0$°C.

Table 2. Effect of Entering Air Humidity Ratio on Bulk Hydraircooling

Case	W_{mae}	Process Time	
		Counterflow	Parallel-flow
1	0.0023	0.3625	0.3482
2	0.0027	0.3607	0.3461
3	0.003	0.3593	0.3445
4	0.0034	0.3582	0.3432
5	0.0037	0.3573	0.3422
6	0.0039	0.3567	0.3416
7	0.0045	0.3552	0.3399
8	0.005	0.3541	0.3387

$T^*_{fe} = 0.156$; $Re_f = 30.0$; $\dot{m}^*_{ma} = 5.0$; $T^*_{mae} = 0.125$; $\lambda^* = 0.6$; $\psi = 0.6$; $L = 10$; $q^*_{int} = 0.003$; $Fr_f = 0.0028$; $\Delta T = 32.0$°C.

Therefore, it can be concluded that T^*_{mae} and W_{mae} do not have any marked effect on the process time.

Figure 14 shows the effect of product-water thermal conductivity ratio (λ^*) on bulk hydraircooling. At first sight, it may appear paradoxical to see that higher thermal conductivity ratios cause lower rates of cooling. This happens because a^* is kept constant and this results in a proportional increase in the thermal capacity of the food product when λ^* is increased. This gives rise to a *prima facie* misleading conclusion that the process time increases with λ^*. However, Figure 15 which is constructed from the dimensional quantities clearly shows that the increase in product thermal conductivity has a favorable effect in terms of the process time. Some actual food products such as apples, grapes and peaches are indicated in the figure to indicate the values of the actual process times.

Figure 16 shows the variation of air and water temperatures along the height of the package for a λ^* of 0.001 ($a^* = 0.0015$) and $q^*_{int} = 0.0$ for both counter- and parallel-flow arrangements at $Fo = 0.0017$ (which corresponds to a dimensional time of 4800s). For such low values of λ^*, the food products may be envisioned as nonconducting insulated spheres, merely serving the purpose of a packing material in a process equipment to

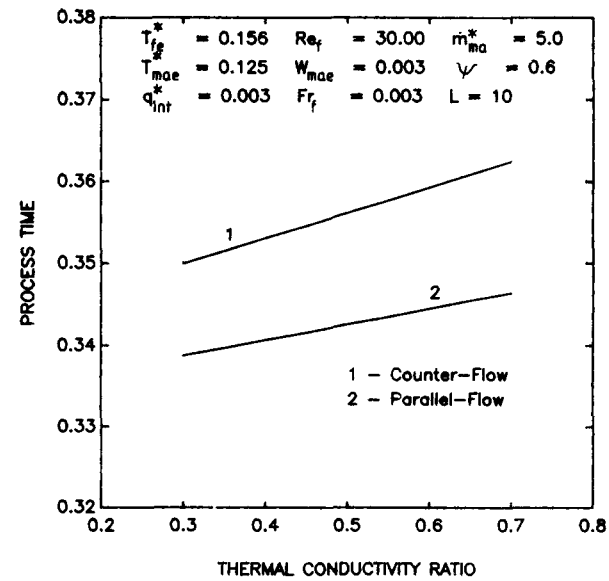

Figure 14. Effect of thermal conductivity ratio on bulk hydraircooling.

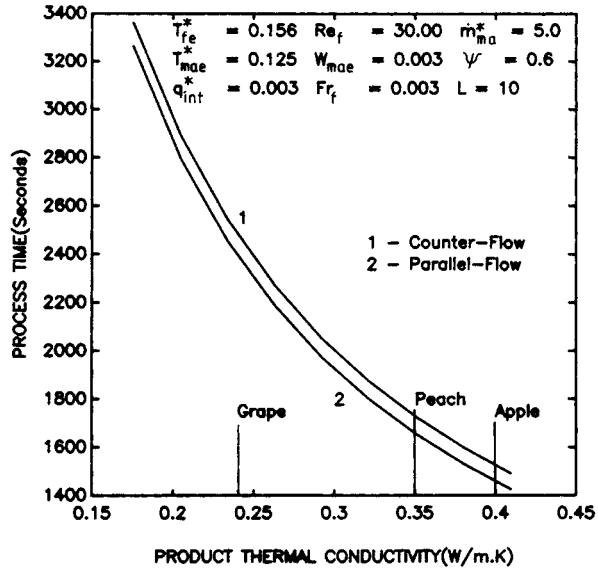

Figure 15. Effect of product thermal conductivity on bulk hydraircooling.

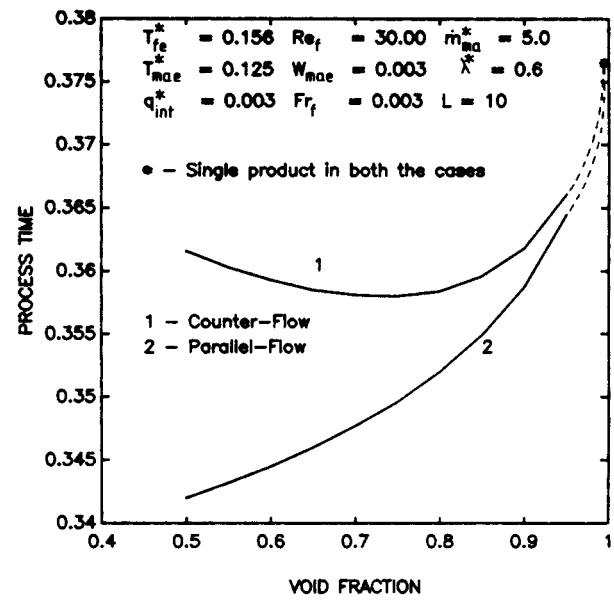

Figure 17. Effect of void fraction on bulk hydraircooling.

enhance the surface area, Thus, the package may now be looked upon as a cooling tower operating in either counterflow or parallel flow. As can be seen from Figure 16, the temperature of the water forming the films and the spray reach relatively lower temperatures in the counterflow than in the parallel-flow arrangement.

Figure 17 shows the effect of void fraction, ψ, on the bulk hydraircooling process. A range of 0.5 to 0.9948 is chosen for void fraction, the former being the void fraction that would result when the products are closely packed in any layer while the latter corresponds to a single product per layer. It can be seen that the process time does not vary much with void fraction. Further, it is also observed that the process time for counterflow process decreases up to a certain value of void fraction and tends to increase slightly for very high values of the void fraction. For parallel flow, process time increases continuously with void fraction. An increase in void fraction means a decrease in the Nusselt and the Sherwood numbers at the film surface (Eq. 35) and hence an increase in the process time. A larger void fraction also implies a smaller number of food products per layer and hence lower heat loads. These two effects result in the trends shown in Figure 17 for counter- and parallel flows. As the void fraction increases, the process time for parallel flow process seems to tend towards that of counterflow process. Process time for single product hydraircooling can be obtained from the present analysis by setting $\psi = 0.9948$, and $L = 1$ (that is, one product layer consisting of one food product). The process time in this case is same for both the processes as depicted in the figure and both the processes appear to approach this value.

The effect of heat of respiration in the product is also studied. As can be seen from Table 3, for the range of the values of heat of respiration rates applicable to common fruits and vegetables, the heat of respiration is not a very important parameter as far as the process time is concerned.

Table 4 shows the process times obtained by varying the Froude number for counter- and cocurrent configurations. The effect of Froude number is not very significant.

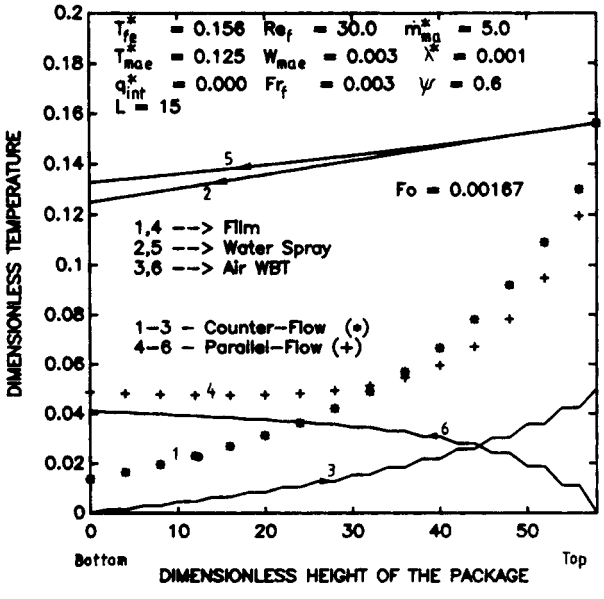

Figure 16. Variation of water and air temperatures as in a cooling tower.

Table 3. Effect of Heat of Respiration on Bulk Hydraircooling

Case	q^*_{int}	Process Time	
		Counterflow	Parallel-flow
1	0.0015	0.3588	0.3441
2	0.003	0.3593	0.3445
3	0.006	0.3602	0.3453
4	0.009	0.3621	0.3461
5	0.012	0.3621	0.3469

$T^*_{fe} = 0.156$; $Re_f = 30.0$; $\dot{m}^*_{ma} = 5.0$; $T^*_{mae} = 0.125$; $W_{mae} = 0.003$; $\lambda^* = 0.6$; $\psi = 0.6$; $L = 10$; $Fr_f = 0.0028$.

Table 4. Effect of Froude Number on Bulk Hydraircooling

Case	Fr_f	Process Time	
		Counterflow	Parallel-flow
1	0.0014	0.3580	0.3445
2	0.0028	0.3593	0.3445
3	0.0042	0.3604	0.3453
4	0.0056	0.3613	0.3460
5	0.0070	0.3622	0.3466

$T^*_{fe}=0.156$; $Re_f=30.0$; $\dot{m}^*_{ma}=5.0$; $T^*_{mae}=0.125$; $W_{mae}=0.003$; $\lambda^*=0.6$; $\psi=0.6$; $L=10$; $q^*_{int}=0.003$.

Table 5 shows the effect of water droplet diameter and its superficial velocity on bulk hydraircooling. The water droplet diameter and its velocity are varied from 0.0004 m to 0.00085 m and 2.5 $m\cdot s^{-1}$ to 10.0 $m\cdot s^{-1}$, respectively. As can be seen from the results, process times vary insignificantly in the case of counterflow and do not vary at all for parallel-flow configuration.

Figure 18 shows the process times for different number of layers in the package for an identical set of processing conditions in counter- and parallel-flow processes. It is observed that the process time is almost the same for packages consisting of up to about 10 product layers. For packages containing more than 10 layers, the process time required is higher for counterflow process than for parallel flow. This is due to the occurrence of an enthalpy cross between the film and the moist air at a certain portion of the package involving some of the top layers as explained earlier. Also, for the given set of parameters, parallel flow ceases to be effective beyond 60 layers where as the counterflow method becomes ineffective beyond 45 layers. These threshold limits for the number of layers beyond which the products cannot reach the storage temperature are indicated in the graph. The saving in terms of process time and also the possibility of precooling larger number of layers using the parallel-flow process result in a higher capacity of the plant compared to counterflow. This conclusion seems to contradict the established fact in case of cooling towers where the counterflow arrangement is supposed to give better

Table 5. Effect of Water Droplet Diameter and its Velocity on Bulk Hydraircooling

Case	d_{wd} (mm)	w_{wd} ($m\cdot s^{-1}$)	Process Time	
			Counterflow	Parallel-flow
1	0.40	2.5	0.3622	0.3446
2	0.40	5.0	0.3612	0.3445
3	0.40	7.5	0.3608	0.3445
4	0.40	10.0	0.3605	0.3445
5	0.55	2.5	0.3612	0.3445
6	0.55	5.0	0.3604	0.3445
7	0.55	7.5	0.3601	0.3445
8	0.55	10.0	0.3599	0.3445
9	0.70	2.5	0.3606	0.3445
10	0.70	5.0	0.3599	0.3445
11	0.70	7.5	0.3597	0.3445
12	0.70	10.0	0.3595	0.3445
13	0.85	2.5	0.3602	0.3445
14	0.85	5.0	0.3596	0.3445
15	0.85	7.5	0.3594	0.3445
16	0.85	10.0	0.3593	0.3445

$T^*_{fe}=0.156$; $Re_f=30.0$; $\dot{m}^*_{ma}=5.0$; $T^*_{mae}=0.125$; $W_{mae}=0.003$; $\lambda^*=0.6$; $\psi=0.6$; $L=10$; $q^*_{int}=0.003$; $Fr_f=0.0028$.

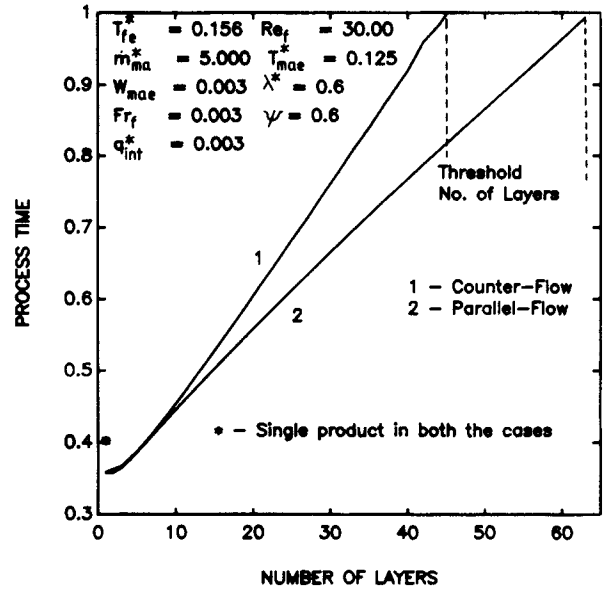

Figure 18. Variation of process time with the number of layers.

performance. However, it should be noted that in a cooling tower the interest is in the final temperatures to which the water is cooled. Even in the present case, the counterflow arrangement yields lower water temperatures as mentioned earlier (Figure 16).

Conclusions

A mathematical model is developed to describe the simultaneous heat and mass transfer occurring during bulk hydraircooling of spherical food products for two different configurations called countercurrent and cocurrent. The governing equations are solved using finite difference numerical methods. A sensitivity analysis is performed to evaluate the effect of each parameter on the process time.

(1) Higher values of film Reynolds number result in faster rates of cooling up to a value of about 20.0.

(2) Higher values of air mass-flow rate yield lower process times up to a value of about 5.0.

(3) Higher values of product thermal conductivity result in faster rates of cooling.

(4) Lower values of entering water temperature yield faster cooling rates.

(5) Process time does not vary significantly with void fraction.

(6) In the range investigated, the heat of respiration within the product is not a very significant parameter.

(7) Parallel-flow hydraircooling process is superior to that of counterflow process, as the former yields higher plant capacities for the same refrigeration capacity.

Notation

a = thermal diffusivity ($m^2\cdot s^{-1}$)
A = area (m^2)
A_0, A_1, A_2 = coefficients defined in Eq. 24
B_0, B_1, B_2 = coefficients defined in Eq. 20
C_0, C_1, C_2 = coefficients defined in Eq. 22
C_p = specific heat ($kJ\cdot kg^{-1}\cdot K^{-1}$)

d = diameter (m)
D = binary diffusion coefficient of water vapor in dry air ($m^2 \cdot s^{-1}$)
D_1-D_4 = coefficients defined in Eq. 37
Fo = Fourier number (dimensionless time)
Fr = Froude number (dimensionless)
g = acceleration due to gravity ($m^2 \cdot s^{-1}$)
h = enthalpy ($kJ \cdot kg^{-1}$)
h_v = enthalpy of water vapor ($kJ \cdot kg^{-1}$)
Δh_v = latent heat of vaporization ($kJ \cdot kg^{-1}$)
H = height of the package (m)
Ja = Jakob number (dimensionless)
L = number of product layers
$\dot{m}$ = mass-flow rate ($kg \cdot s^{-1}$)
Nu = Nusselt number (dimensionless)
Pr = Prandtl number (dimensionless)
q_{int} = heat of respiration in the food product ($W \cdot m^{-3}$)
r = radial coordinate
R = radius of the spherical food product (m)
R_m = mass fraction ratio (dimensionless)
R_T = temperature ratio (dimensionless)
Re = Reynolds number (dimensionless)
Re_{mwd} = modified water droplet Reynolds number (dimensionless)
S_1-S_4 = coefficients defined in Eq. 60
Sc = Schmidt number (dimensionless)
Sh = Sherwood number (dimensionless)
t = time (s)
T = temperature (°C)
v_θ = tangential velocity in the film ($m \cdot s^{-1}$)
w = average velocity ($m \cdot s^{-1}$)
W = humidity ratio (kg/kg of dry air)
y = radial coordinate in the film
z = coordinate along the height of the package

Greek letters

α_h = heat-transfer coefficient ($W \cdot m^{-2} \cdot K^{-1}$)
α_m = mass-transfer coefficient ($kg \cdot m^{-2} \cdot s^{-1}$)
δ = film thickness (m)
θ = angular coordinate
λ = thermal conductivity ($W \cdot m^{-1} \cdot K^{-1}$)
μ = dynamic viscosity ($N \cdot s \cdot m^{-2}$)
ν = kinematic viscosity ($m^2 \cdot s^{-1}$)
ρ = density ($kg \cdot m^{-3}$)
ψ = void fraction (dimensionless)

Subscripts

c = cross-section
e = entry
f = water
fbm = fluid bulk mean
ff = water film
ffp = water film over food product
i = interstitial
ma = moist air
o = initial
p = product
s = saturated, superficial
u = per unit volume of the package (m^{-3})
wb = wet bulb
wd = water droplet

Superscripts

*,** = dimensionless quantity

Literature Cited

Abdul Majeed, P. M., "Analysis of Heat Transfer During Hydraircooling of Spherical Food Products," *Int. J. Heat Mass Transfer*, **24**, 323 (1984).

ASHRAE Guide and Data Book (Applications), Amer. Soc. of Heating, Refrigerating and Air Conditioning Engineers, Atlanta (1971).

ASHRAE Handbook (Fundamentals), Amer. Soc. of Heating, Refrigerating and Air Conditioning Engineers, Atlanta (1989).

Beukema, K. J., S. Bruin, and J. Schenk, "Heat and Mass Transfer During Cooling and Storage of Agricultural Products," *Chem. Eng. Sci.*, **37**, 291 (1982).

Bird, R. B., W. E. Stewart, and E. N. Lightfoot, *Transport Phenomena*, Wiley, New York (1960).

Carslaw, H. S., and J. C. Jaeger, *Conduction of Heat in Solids*, 2nd ed., Oxford at the Clarendon Press (1959).

Chyu, M. C., and A. H. Bergles, "An Analytical and Experimental Study of Falling-Film Evaporation on a Horizontal Tube," *Trans. ASME, J. Heat Transfer*, **109**, 983 (1987).

Gaffney, J. J., C. D. Baird, and K. V. Chau, "Methods for Calculating Heat and Mass Transfer in Fruits and Vegetables Individually and in Bulk," *ASHRAE Trans.*, **91**, Part 2B, 332 (1985).

Hall, E. G., "Techniques of Precooling, the Long Term Storage, C. A. Storage and the Freezing of Fruits and Vegetables: I: Precooling of Fruit and Vegetables," Int. Short Term Course, Durgapur, India, F. A. O.-I. I. R., 75 (Jan. 14-24, 1974).

Holman, J. P., *Heat Transfer*, 6th ed., McGraw-Hill, Singapore (1986).

Hwang, G. J., and K. C. Cheng, "Boundary Vorticity Method for Convective Heat Transfer with Secondary Flow—Application to the Combined Free and Forced Laminar Convection in Horizontal Tubes," *Proc. Int. Heat Transfer Conf.*, Paris-Versailles, Vol. IV, Paper NC 3.5, Elsevier, Amsterdam (1970).

Krishna Murthy, M. V., and K. Badarinarayana, "Heat Transfer in Food Products," VI Int. Heat Transfer Conference, Toronto, Canada, **6**. p. 339 (Aug. 7-11, 1978).

Lamberg, I., and B. Hallstrom, "Thermal Properties of Potatoes and a Computer Simulation of a Blanching Process," *J. Food Tech.*, **21**, 577 (1986).

Peaceman, R. W., and H. H. Rachford, "The Numerical Solutions of Parabolic and Elliptic Equations," *J. Soc. Ind. Appl. Math.*, **3**, 28 (1955).

Ranz, W. E., and W. R. Marshall, "Evaporation From Drops: I," *Chem. Eng. Prog.*, **48**, 141 (1952).

Roache, P. J., *Computational Fluid Dynamics*, Revised English edition, Hermosa Publishers, Albuquerque, NM (1982).

Soule, J., G. E. Yost, and A. H. Bennett, "Certain Heat Transfer Characteristics of Oranges, Grapefruit and Tangelos During Forced-Air Precooling," *Trans. ASAE*, **9**, 355 (1966).

von Rosenberg, D. U., *Methods for the Numerical Solution of Partial Differential Equations*, Elsevier, New York (1969).

Manuscript received June 2, 1992, and revision received March 1, 1993.